Nuclear Mathematical and Computational Sciences: A Century in Review, A Century Anew
Gatlinburg, Tennessee, April 6-11, 2003, on CD-ROM, American Nuclear Society, LaGrange Park, IL (2003)

A VARIATIONAL P_1-DP_0 DIFFUSION THEORY FOR PLANAR GEOMETRY

Patrick S. Brantley
Lawrence Livermore National Laboratory
P.O. Box 808, L-23
Livermore, CA 94551
brantley1@llnl.gov

ABSTRACT

A variational analysis is used to derive a mixed P_1-DP_0 (spherical harmonics–double spherical harmonics) angular approximation to the time-independent monoenergetic neutron transport equation with linearly anisotropic scattering in one-dimensional planar geometry. This mixed approximation contains a space-dependent weight factor $\alpha(x)$ that controls the local angular approximation used: $\alpha(x) = 1$ yields the standard P_1 (diffusion) approximation, $\alpha(x) = 0$ gives the standard DP_0 approximation, and $0 < \alpha(x) < 1$ produces a mixed approximation. The diffusion equation obtained differs from the standard P_1 diffusion equation only in the definition of the diffusion coefficient. The variational analysis shows that both the scalar flux and the current are continuous at material interfaces regardless of the value of $\alpha(x)$. Standard Marshak boundary conditions are also obtained via the variational analysis. In this paper, we examine the use of this mixed angular approximation to more accurately treat material interfaces and vacuum boundaries. Numerical results from a mixed-oxide fuel test problem are presented to demonstrate that significant improvements in accuracy can be obtained using this method. For this test problem, the mixed P_1-DP_0 angular approximation with $\alpha = 0.25$ is found to be more robust than the standard DP_0 approximation ($\alpha = 0$) for treating the material interfaces and vacuum boundaries.

Key Words: neutron transport, spherical harmonics approximation, double spherical harmonics approximation, variational analysis, mixed-oxide fuel

1. INTRODUCTION

The spherical harmonics (P_N) and double spherical harmonics (DP_N) angular approximations to the planar-geometry neutron transport equation are well established [1]. In the P_N approximation, the angular dependence ($-1 \leq \mu \leq 1$) of the neutron angular flux is expanded in a truncated Legendre polynomial series that is continuous at all spatial points. However, the angular flux at an internal material interface or at a vacuum boundary is discontinuous at $\mu = 0$ when viewed as a function of angle [2]. Therefore, the P_N approximation may give a poor representation of the angular flux at these discontinuities unless a high order approximation is used. The desire to more accurately treat these discontinuities with low order approximations motivated the development of the DP_N approximation. In the DP_N approximation, the angular dependence of the neutron angular flux is expanded in separate Legendre polynomial expansions over the half angular ranges $-1 \leq \mu < 0$ and $0 < \mu \leq 1$. As a result, the DP_N approximation can more accurately capture the discontinuity in the angular flux at material interfaces and at vacuum boundaries. While the DP_N approximation offers the possibility of more accurately treating material interfaces and vacuum boundaries, its use as a practical numerical tool has been limited. The current lack of use is due at least in part to the inapplicability of the DP_N approximation with $N > 0$ to multi-dimensional geometries.

Paveri-Fontana and Amster [3] extended the DP_0 approximation to multi-dimensional geometries using both a generalization of the usual derivation of the DP_0 approximation as well as a variational analysis. Their variational analysis considered only the interior of the system (i.e. no material interface or boundary terms were included in their variational functional); they proposed material interface and boundary conditions based on physical arguments. The diffusion equation they derived for the DP_0 approximation differed from the standard P_1 diffusion equation only in the value of the diffusion coeffi cent. The paper [3] discusses only the use of either the P_1 *or* the DP_0 approximation in a given region, and no numerical results were presented to demonstrate the accuracy of the method.

Demény et al. [4] suggested the use of a DP_N approximation at vacuum boundaries *coupled* with a P_N approximation in the interior of a system to improve the accuracy of computed escaping neutron angular distributions at a boundary. Their P_N-DP_N Marshak-like boundary conditions were obtained in a heuristic manner. Nonetheless, they found that extrapolation values computed for the Milne problem converged to the exact value more rapidly with the order of the angular approximation when the DP_N approximation was utilized at the boundary. In addition, the escaping neutron angular distributions were generally more accurate with the use of the DP_N boundary condition.

In this paper, we derive a mixed P_1-DP_0 angular approximation to the time-independent monoenergetic neutron transport equation with linearly anisotropic scattering in one-dimensional planar geometry. Our analysis is based on a variational functional which includes both material interface and boundary terms [2]. The forward and adjoint trial functions utilized in the variational analysis are motivated by the work of Paveri-Fontana and Amster [3] and Gelbard et al. [5]. We include a weighted average of the P_1 and DP_0 angular approximations in our trial function. This mixed angular approximation contains a user-prescribed space-dependent weight factor $\alpha(x)$ that controls the local angular approximation used: $\alpha(x) = 1$ yields the standard P_1 (diffusion) approximation, $\alpha(x) = 0$ gives the standard DP_0 approximation, and $0 < \alpha(x) < 1$ produces a mixed approximation. As in the work of Paveri-Fontana and Amster, the diffusion theory obtained from our variational analysis differs from the standard P_1 diffusion theory only in the value of the diffusion coeffi cient. [We note that for $\alpha(x) = 1$, our diffusion theory is identical with standard diffusion theory.] Therefore, the mixed P_1-DP_0 diffusion theory requires essentially the same computational effort as standard P_1 diffusion theory. Although we consider only planar geometry in this paper, we believe our analysis can be extended to multi-dimensional geometries using the methodology of Paveri-Fontana and Amster.

Although potentially much broader in application, we examine in this paper the use of this mixed P_1-DP_0 approximation to more accurately treat both material interfaces and vacuum boundaries. Our approach is to use the P_1 approximation everywhere in the system except possibly at material interfaces and/or vacuum boundaries. The DP_0 or a mixed P_1-DP_0 approximation with $0 < \alpha(x) < 1$ is used within the order of a mean free path (mfp) around material interfaces and near vacuum boundaries. Our numerical results demonstrate that this method can signifi cantly improve accuracy near these material interfaces and vacuum boundaries. In particular, we apply this methodology to a mixed-oxide fuel test problem that possesses signifi cant material property discontinuities.

The remainder of this paper is organized as follows. In Section 2, we outline the variational derivation of the mixed P_1-DP_0 approximation. Next, we present numerical results from a mixed-oxide test problem in Section 3. We offer concluding remarks and suggestions for future work in Section 4.

2. VARIATIONAL ANALYSIS

In this section, we outline the variational derivation of the mixed P_1-DP_0 approximation for a piecewise homogeneous medium. We consider a system V consisting of I homogeneous slab material regions V_i $(1 \leq i \leq I)$ with boundaries at $x = 0$ and $x = L$ and internal material interfaces

$$\partial V_{ij} = V_i \bigcap V_j \ . \tag{1}$$

We consider the following time-independent monoenergetic neutron transport problem with linearly anisotropic scattering in the one-dimensional system V:

$$\mu \frac{\partial}{\partial x} \Psi(x,\mu) + \sigma_t^i \Psi(x,\mu) = \int_{-1}^{1} \sigma_s^i(\mu,\mu') \Psi(x,\mu') \, d\mu' + \frac{1}{2} Q(x) \ , \ x \in V_i \ , \ -1 \leq \mu \leq 1 \ , \tag{2}$$

$$\lim_{\epsilon \to 0^+} \Psi(x + \epsilon\mu, \mu) = \lim_{\epsilon \to 0^+} \Psi(x - \epsilon\mu, \mu) \ , \ x \in \partial V_{ij} \ , \tag{3}$$

$$\Psi(0,\mu) = \Psi^0(\mu) \ , \ 0 < \mu \leq 1 \ , \tag{4}$$

$$\Psi(L,\mu) = \Psi(L,-\mu) \ , \ -1 \leq \mu < 0 \ , \tag{5}$$

where the differential scattering cross section is given by

$$\sigma_s^i(\mu,\mu') = \frac{1}{2}\sigma_{s0}^i + \frac{3}{2}\sigma_{s1}^i \mu\mu' \ , \tag{6}$$

and $\Psi^0(\mu)$ is a prescribed incident angular flux. The notation in Eqs. (2)–(5) is standard neutronics notation. For the transport problem Eqs. (2)–(5), we would like to calculate the scalar functional $\mathcal{I}$ defined as

$$\mathcal{I}[\Psi] = \sum_{i=1}^{I} \int_{V_i} \int_{-1}^{1} \sigma^*(x) \Psi(x,\mu) \, d\mu dx \ , \tag{7}$$

where $\sigma^*(x)$ is a prescribed function. If $\sigma^*(x)$ is a physical cross section in material zone V_i and zero elsewhere, then the functional $\mathcal{I}$ represents the corresponding reaction rate in material zone V_i.

To variationally approximate $\mathcal{I}[\Psi]$, we consider the associated functional $\mathcal{J}[\psi, \psi^*]$ defined by [2]:

$$\begin{aligned} \mathcal{J}[\psi,\psi^*] &= \mathcal{I}[\psi] \\ &- \sum_{i=1}^{I} \int_{V_i} \int_{-1}^{1} \psi^* \left[\mu \frac{\partial}{\partial x}\psi + \sigma_t^i \psi - \int_{-1}^{1} \sigma_s^i(\mu,\mu') \psi(x,\mu') \, d\mu' - \frac{1}{2} Q(x) \right] d\mu dx \\ &+ \frac{1}{2} \sum_{i=1}^{I-1} \int_{-1}^{1} \mu \left(\psi^{*i} + \psi^{*i+1} \right) \left(\psi^i - \psi^{i+1} \right) d\mu \\ &- \int_0^1 \mu \left[\psi^*(0,\mu) + \psi^*(0,-\mu) \right] \left[\psi(0,\mu) - \Psi^0(\mu) \right] d\mu \\ &+ \int_{-1}^{0} \mu \psi^*(L,\mu) \left[\psi(L,\mu) - \psi(L,-\mu) \right] d\mu \ . \end{aligned} \tag{8}$$

Here we have denoted by ψ^i and ψ^{*i} the values

$$\psi^{(*)i}(x,\mu) = \begin{cases} \lim_{\epsilon \to 0^+} \psi^{(*)}(x + \epsilon\mu, \mu) \ , \ x \in \partial V_{ij} \ , \ -1 \leq \mu < 0 \ , \\ \lim_{\epsilon \to 0^+} \psi^{(*)}(x - \epsilon\mu, \mu) \ , \ x \in \partial V_{ij} \ , \ \ 0 < \mu \leq 1 \ , \end{cases} \tag{9}$$

i.e. the functions $\psi(x,\mu)$ and $\psi^*(x,\mu)$ at the point x in an ϵ-neighborhood of the internal material interface ∂V_{ij}, but in material zone V_i. The variational functional $\mathcal{J}$ is a one-dimensional planar-geometry version of a functional previously used to derive multi-dimensional P_1 [6] and simplified P_N [7] approximations.

We can readily show that the functional $\mathcal{J}$ has the following properties:

1. If $\psi = \Psi$, where Ψ satisfies the forward transport problem given by Eqs. (2)–(5), then $\mathcal{J} = \mathcal{I}$ for any choice of ψ^*.
2. If $\psi = \Psi + \delta\Psi$ and $\psi^* = \Psi^* + \delta\Psi^*$, where Ψ satisfies the forward transport problem Eqs. (2)–(5), Ψ^* is an arbitrary function, and $\delta\Psi$ and $\delta\Psi^*$ represent small but arbitrary $O(\delta)$ variations, then $\mathcal{J} = \mathcal{I} + O(\delta)$.
3. If $\psi = \Psi + \delta\Psi$ and $\psi^* = \Psi^* + \delta\Psi^*$, where Ψ satisfies the forward transport problem Eqs. (2)–(5), Ψ^* satisfies the adjoint transport problem given by

$$-\mu\frac{\partial}{\partial x}\Psi^*(x,\mu) + \sigma_t^i\Psi^*(x,\mu) = \int_{-1}^{1}\sigma_s^i(\mu,\mu')\,\Psi^*(x,\mu')\,d\mu' + \sigma^*(x) \;\;,\;\; x \in V_i \;\;, \tag{10}$$

$$\lim_{\epsilon\to 0^+}\Psi^*(x+\epsilon\mu,\mu) = \lim_{\epsilon\to 0^+}\Psi^*(x-\epsilon\mu,\mu) \;\;,\;\; x \in \partial V_{ij} \;\;, \tag{11}$$

$$\Psi^*(0,\mu) = 0 \;\;,\;\; -1 \le \mu < 0 \;\;, \tag{12}$$

$$\Psi^*(L,\mu) = \Psi^*(L,-\mu) \;\;,\;\; 0 < \mu \le 1 \;\;, \tag{13}$$

   and $\delta\Psi$ and $\delta\Psi^*$ represent small but arbitrary $O(\delta)$ variations, then $\mathcal{J} = \mathcal{I} + O(\delta^2)$.

Thus, given approximations to the forward and adjoint angular fluxes, Ψ and Ψ^*, that have errors of $O(\delta)$, the functional $\mathcal{J}$ approximates the functional $\mathcal{I}$ with an error of $O(\delta^2)$. In the language of the calculus of variations, the functional $\mathcal{J}$, Eq. (8), is a Lagrangian function for the system and Eqs. (2)–(5) and Eqs. (10)–(13) are the Euler equations [2].

The results above imply that $\psi = \Psi$ and $\psi^* = \Psi^*$ is the only stationary point of the functional $\mathcal{J}$. The requirement that the functional $\mathcal{J}$ be stationary for small but arbitrary variations in Ψ and Ψ^* is equivalent to the forward and adjoint transport problems, Eqs. (2)–(5) and Eqs. (10)–(13). Only the true forward and adjoint transport solutions can exactly satisfy this requirement. However, if we assume approximate forms (trial functions) for the forward and adjoint solutions and require that the functional be stationary with respect to variations of these approximate functions, then equations can be derived that yield approximate solutions to the forward and adjoint transport problems.

It should be noted that the term $\psi^*(0,-\mu)$ in the boundary term of Eq. (8) can be dropped, and the functional $\mathcal{J}$ remains an $O(\delta^2)$ approximation to $\mathcal{I}$ provided $\psi = \Psi + O(\delta)$ and $\psi^* = \Psi^* + O(\delta)$. However, including this term leads to a simpler analysis that yields Marshak-like boundary conditions; excluding it leads to different (non-Marshak) boundary conditions. (This was initally observed in the variational derivation of the P_1 approximation to general-geometry multigroup transport problems by Rulko et al. [6].)

To proceed with the variational analysis, we must formulate approximate forms (trial functions) for the forward and adjoint angular flux. The P_1 representation of the forward angular flux is given by [2]

$$\Psi(x,\mu) = \frac{1}{2}\Phi_0(x) + \frac{3}{2}\mu\Phi_1(x) \;\;,\;\; -1 \le \mu \le 1 \;\;, \tag{14}$$

where $\Phi_0(x)$ is the neutron scalar flux and $\Phi_1(x)$ is the neutron current. Thus, the P_1 representation of the angular flux is linearly anisotropic in angle. The DP_0 representation of the angular flux is given by [2]

$$\Psi(x,\mu) = \begin{cases} \Psi^+(x) \ , & 0 < \mu \leq 1 \ , \\ \Psi^-(x) \ , & -1 \leq \mu < 0 \ . \end{cases} \tag{15}$$

Thus, the DP_0 representation of the angular flux is isotropic in angle in each of the half angular ranges $-1 \leq \mu < 0$ and $0 < \mu \leq 1$. Following Paveri-Fontana and Amster [3] and Gelbard et al. [5], we note that $\Phi_0(x) = \Psi^+(x) + \Psi^-(x)$ and $\Phi_1(x) = \frac{1}{2}[\Psi^+(x) - \Psi^-(x)]$. Then we can rewrite Eq. (15) as

$$\Psi(x,\mu) = \frac{1}{2}\Phi_0(x) + \frac{3}{2} f(\mu)\Phi_1(x) \ , \ -1 \leq \mu \leq 1 \ , \tag{16}$$

where the function $f(\mu)$ is given by

$$f(\mu) = \begin{cases} \frac{2}{3} \ , & 0 < \mu \leq 1 \ , \\ -\frac{2}{3} \ , & -1 \leq \mu < 0 \ . \end{cases} \tag{17}$$

The forward trial function for the angular flux that we use in our variational analysis is a weighted average of the P_1 and the DP_0 representations, Eqs. (14) and (16), which we refer to as a mixed P_1-DP_0 approximation. This trial function is given by

$$\psi(x,\mu) = \frac{1}{2}\phi_0(x) + \frac{3}{2} K(x,\mu)\phi_1(x) \ , \ -1 \leq \mu \leq 1 \ , \tag{18}$$

where the function $K(x,\mu)$ is given by

$$K(x,\mu) = \begin{cases} \frac{2}{3}[1-\alpha(x)] + \alpha(x)\mu \ , & 0 < \mu \leq 1 \ , \\ -\frac{2}{3}[1-\alpha(x)] + \alpha(x)\mu \ , & -1 \leq \mu < 0 \ , \end{cases} \tag{19}$$

and $0 \leq \alpha(x) \leq 1$ is a user-prescribed space-dependent weight factor. For $\alpha(x) = 1$, Eq. (18) is equivalent to the P_1 approximation, and for $\alpha(x) = 0$ it is equivalent to the DP_0 approximation. Setting $0 < \alpha(x) < 1$ yields an intermediate approximation. For the adjoint trial function, we use an analogous form:

$$\psi^*(x,\mu) = \frac{1}{2}\phi_0^*(x) + \frac{3}{2} K(x,\mu)\phi_1^*(x) \ , \ -1 \leq \mu \leq 1 \ . \tag{20}$$

Inserting the trial functions, Eqs. (18) and (20), into the functional $\mathcal{J}$ and performing all possible angular integrations, we obtain the following reduced form of $\mathcal{J}$:

$$\begin{aligned} &\mathcal{J}[\phi_0(x), \phi_1(x), \phi_0^*(x), \phi_1^*(x)] = \\ &\sum_{i=1}^{I} \int_{V_i} \sigma^*(x)\phi_0(x)\,dx \\ &-\frac{1}{2}\sum_{i=1}^{I} \int_{V_i} \phi_0^*(x)\left[\frac{d}{dx}\phi_1(x) + \sigma_{a0}^i \phi_0(x) - Q(x)\right] dx \\ &-\frac{3}{2}\sum_{i=1}^{I} \int_{V_i} \phi_1^*(x)\left[\frac{1}{3}\frac{d}{dx}\phi_0(x) + \widehat{\sigma_{a1}^i}(x)\phi_1(x)\right] dx \\ &+\frac{1}{4}\sum_{i=1}^{I-1}\left[\phi_0^{*i}(x) + \phi_0^{*i+1}(x)\right]\left[\phi_1^i(x) - \phi_1^{i+1}(x)\right] \end{aligned}$$

$$+\frac{1}{4}\sum_{i=1}^{I-1}\left[\phi_1^{*i}(x)+\phi_1^{*i+1}(x)\right]\left[\phi_0^{i}(x)-\phi_0^{i+1}(x)\right]$$
$$-\phi_0^*(0)\left[\frac{1}{4}\phi_0(0)+\frac{1}{2}\phi_1(0)-\int_0^1\mu\Psi^0(\mu)\,d\mu\right]$$
$$+\left\{\frac{1}{2}\phi_0^*(L)-\left[\left(1-(\alpha(L))^2\right)+\frac{9}{8}(\alpha(L))^2\right]\phi_1^*(L)\right\}\phi_1(L)\ , \tag{21}$$

where

$$\sigma_{a0}^i=\sigma_t^i-\sigma_{s0}^i\ , \tag{22}$$

and

$$\widehat{\sigma_{a1}^i}(x)=\left\{\frac{4}{3}[1-\alpha(x)]^2+2[1-\alpha(x)]\alpha(x)+[\alpha(x)]^2\right\}\sigma_t^i-\sigma_{s1}^i\ . \tag{23}$$

If we calculate the first variation $\delta\mathcal{J}$ of the reduced functional $\mathcal{J}$ with respect to independent variations of the unknown functions $\delta\phi_0^*(x)$ and $\delta\phi_1^*(x)$ and set this equal to zero, we obtain the forward P_1-DP_0 equations

$$\frac{d}{dx}\phi_1(x)+\sigma_{a0}^i\phi_0(x)=Q(x)\ ,\ \ x\in V_i\ , \tag{24}$$

and

$$\frac{1}{3}\frac{d}{dx}\phi_0(x)+\widehat{\sigma_{a1}^i}(x)\,\phi_1(x)=0\ ,\ \ x\in V_i\ , \tag{25}$$

with material interface conditions

$$\phi_0^i(x)=\phi_0^{i+1}(x)\ \ ,\ \ x\in\partial V_{i,i+1}\ , \tag{26}$$

$$\phi_1^i(x)=\phi_1^{i+1}(x)\ \ ,\ \ x\in\partial V_{i,i+1}\ , \tag{27}$$

a Marshak boundary condition at $x=0$,

$$\frac{1}{4}\phi_0(0)+\frac{1}{2}\phi_1(0)=\int_0^1\mu\Psi^0(\mu)\ \ , \tag{28}$$

and the reflecting boundary condition at $x=L$

$$\phi_1(L)=0\ . \tag{29}$$

Eqs. (26) and (27) demonstrate that the scalar flux and current are continuous at a material interface for any value of the weight factor $\alpha(x)$.

Eqs. (24)–(29) can be rewritten as a diffusion theory by eliminating $\phi_1(x)$ to obtain

$$-\frac{d}{dx}D^i(x)\frac{d}{dx}\phi_0(x)+\sigma_{a0}^i\phi_0(x)=Q(x)\ ,\ \ x\in V_i\ , \tag{30}$$

with the material interface conditions

$$\phi_0^i(x)=\phi_0^{i+1}(x)\ \ ,\ \ x\in\partial V_{i,i+1}\ , \tag{31}$$

$$D^i(x)\frac{d}{dx}\phi_0^i(x)=D^{i+1}(x)\frac{d}{dx}\phi_0^{i+1}(x)\ \ ,\ \ x\in\partial V_{i,i+1}\ , \tag{32}$$

a Marshak boundary condition at $x = 0$,

$$\frac{1}{4}\phi_0(0) - \frac{1}{2}D^1(0)\frac{d}{dx}\phi_0(0) = \int_0^1 \mu\Psi^0(\mu)\,d\mu \ , \tag{33}$$

and the reflecting boundary condition at $x = L$,

$$\frac{d}{dx}\phi_0(L) = 0 \ , \tag{34}$$

where the diffusion coefficient $D^i(x)$ is given by

$$D^i(x) = \frac{1}{3\widehat{\sigma^i_{a1}(x)}} \ , \ x \in V_i \ . \tag{35}$$

The expression for the diffusion coefficient given by Eq. (35) interpolates quadratically [in $\alpha(x)$] between the DP_0 and the P_1 values of the diffusion coefficient. Eqs. (30)–(35) are identical to standard P_1 diffusion theory with the exception of a slightly different diffusion coefficient [for $\alpha(x) < 1$]. Thus, the mixed P_1-DP_0 diffusion approximation can be readily solved numerically using standard diffusion discretizations and solvers with essentially no additional computational expense.

3. NUMERICAL RESULTS

In this section, we apply the mixed P_1-DP_0 approximation derived in Section 2 to a mixed-oxide (MOX) fuel test problem. MOX fuel assemblies possess significantly different neutronic properties than UO_2 fuel assemblies [7]. Namely, the thermal absorption and fission cross sections in MOX assemblies are much higher than in UO_2 assemblies. As a result, the thermal flux is much lower in the MOX assemblies as compared to the UO_2 assemblies, while the power production is much higher. The stronger absorption in MOX assemblies and the large cross section discontinuities at MOX/UO_2 assembly interfaces can be challenging for the diffusion approximation.

Our one-group fixed-source test problem has two material regions whose cross sections are representative of the thermal group of mixed-oxide and UO_2 fuel assemblies. This one-dimensional test problem is based on the multi-dimensional OECD/NEACRP-L-336 C5 mixed-oxide benchmark problem proposed by the Nuclear Energy Agency Committee on Reactor Physics [8]. The geometry is shown in Figure 1, where the dimensions of the "assemblies" correspond to those specified in the benchmark. The assembly-homogenized cross section values were obtained by homogenization of the specified pin cell cross sections [7] and are given in Table I. We note that this test problem includes only isotropic scattering. The higher power production in the MOX fuel region is represented as a larger fixed source value.

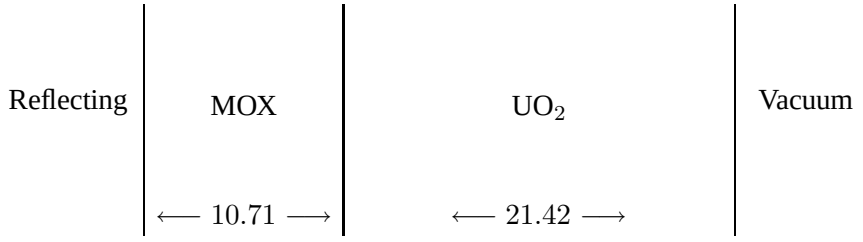

Figure 1. MOX Test Problem Configuration

Table I. Test Problem Material Properties

Region	σ_t	σ_s	σ_a	Q
MOX	0.83333	0.60272	0.23061	1.0
UO_2	0.83333	0.74091	0.09242	0.65

We use this test problem to assess the improvement in accuracy that can be obtained using the mixed P_1-DP_0 approximation at material interfaces and vacuum boundaries. Since we are interested in assessing the accuracy improvement obtained using our mixed *angular* approximation, we simulate this problem using a fine spatial mesh of less than 0.001 mfp per zone to minimize *spatial* discretization errors. We compare the computed scalar flux values to a reference P_{15} solution obtained using a very fine spatial mesh of less than 0.0001 mfp per zone. To evaluate the error in the computed solution, we compute the root-mean-squared (RMS) relative error in the scalar flux across several edit regions of the problem: the total problem, the interior of the left MOX region, the interior of the right UO_2 region, 3 mfp on either side of the MOX/UO_2 interface, and 3 mfp near the vacuum boundary. In addition, we compute the error in the absorption rate for both the MOX and the UO_2 regions. The accurate computation of the reaction rate in each region is important, since the reaction rate in a region is often the desired result (e.g. for determining the power production).

We plot the standard P_1 scalar flux and the reference P_{15} scalar flux in Figure 2 along with the percent relative error in the P_1 scalar flux in Figure 3. We note that the error in the P_1 scalar flux in the interior of each region (away from the material interface and the vacuum boundary) is small. The error in the P_1 scalar flux near the material interface between the MOX and the UO_2 region and near the vacuum boundary is evident. The relative errors approach 1-2% near the material interface and near the vacuum boundary are as large as 10%. The edit region RMS relative errors for the standard P_1 approximation [$\alpha(x) = 1$ for all x] with Marshak vacuum boundary conditions are given in Table II. The errors range from a few hundredths of a percent in the interior of the MOX and UO_2 regions to approximately one percent near the vacuum boundary. The total error is dominated by the error near the material interface and the vacuum boundary. The errors in the interior of the MOX and UO_2 regions are significantly smaller than near the material interface and the vacuum boundary.

In Table III, we give the percent relative error in the absorption rate (compared to the reference P_{15} solution) for the P_1 approximation. The P_1 approximation over-predicts the absorption rate in the MOX region by about 0.1% and underpredicts the absorption rate in the UO_2 region by about 0.3%.

We next present a series of calculations in which we treat the MOX/UO_2 material interface and the vacuum boundary using the mixed P_1-DP_0 angular approximation. For simplicity, we simultaneously vary the width of the mixed P_1-DP_0 region from 0 to 2 mfp on each side of the material interface and from 0 to 2 mfp near the vacuum boundary. We treat the mixed approximation region as either an average of the P_1 and DP_0 approximations (with $\alpha = 0.5$ and 0.25) or as the standard DP_0 approximation ($\alpha = 0$). For each edit region, we compute an error reduction factor (ERF) defined as the ratio of the RMS relative error in the edit region for the given angular approximation to the standard P_1 RMS relative error in the edit region. Therefore, a small value for the ERF is desirable; an ERF greater than unity implies that the error actually increased. We also define the set of optimal ERFs as the set with the smallest weighted average ERF, where each edit region ERF is weighted by the error in the region to determine the average.

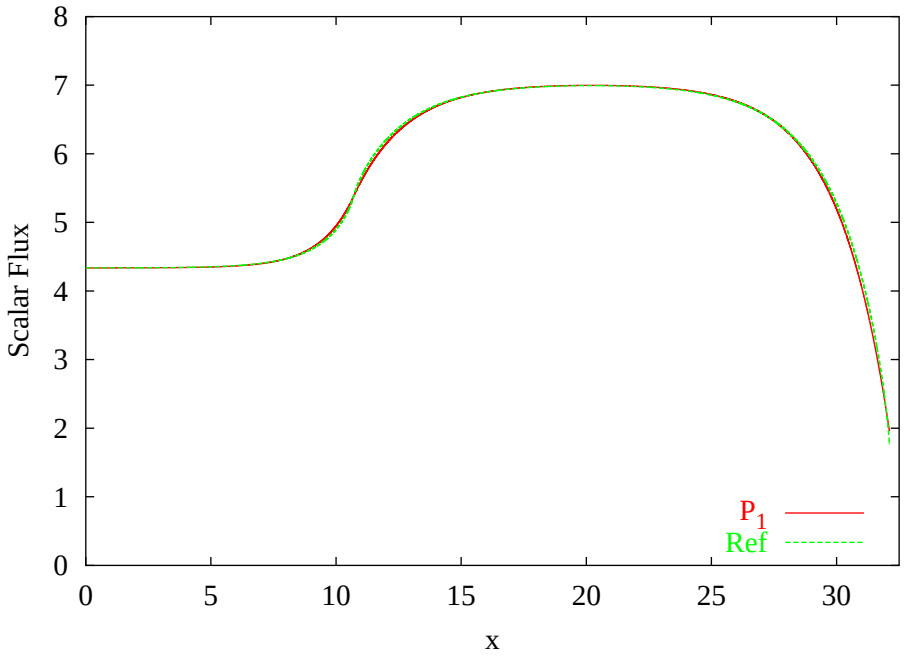

Figure 2. Scalar Flux for P_1 Approximation

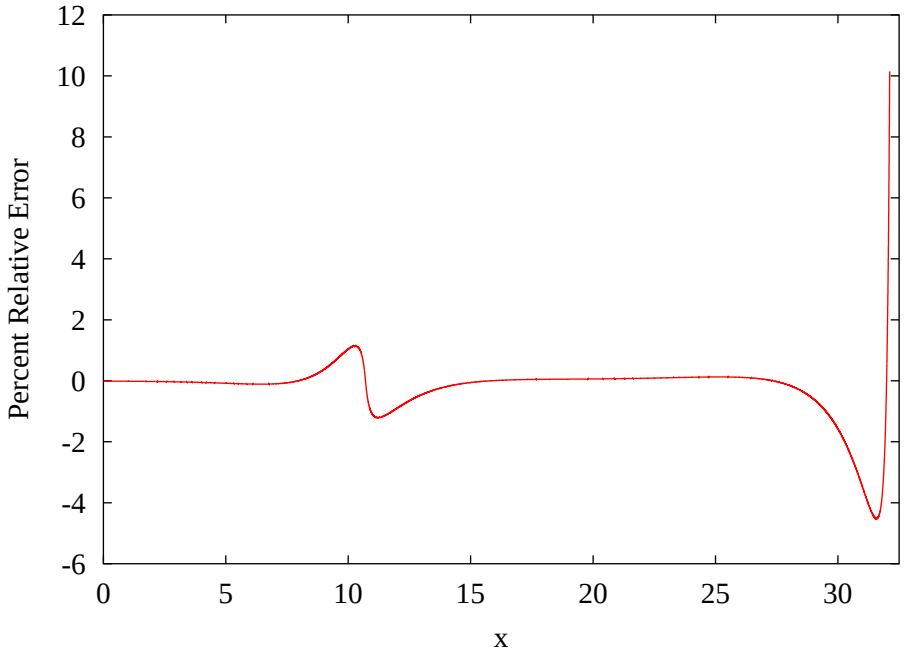

Figure 3. Scalar Flux Error for P_1 Approximation

Figures 4 and 5 plot the RMS relative error in the scalar flux for the mixed P_1-DP_0 angular approximation with $\alpha(x) = 0.5$ and $\alpha(x) = 0.25$ in the mixed region, respectively, for each of the five edit regions as a function of the number of mfp in the mixed regions. A mixed region width of zero corresponds to the standard P_1 case. In each case, the curves exhibit the same general trends. Namely, the total error and the

Table II. Standard P_1 Approximation Errors and Optimal Error Reduction Factors

Region	P_1 RMS Percent Relative Error in Scalar Flux	Optimal Error Reduction Factors		
		$\alpha(x)$ = 0.5	$\alpha(x)$ = 0.25	$\alpha(x)$ = 0.0
Total	0.9542	0.667	0.434	0.424
MOX	0.0302	1.238	1.318	1.328
UO_2	0.0603	1.295	1.532	1.566
Interface	0.3174	0.640	0.402	0.311
Boundary	0.8973	0.666	0.424	0.422
	Optimal mixed width (mfp)	0.700	0.400	0.225

Table III. Regional Absorption Rates and Percent Relative Errors

Region	Exact Rate	Percent Relative Error in Absorption Rate			
		P_1	$\alpha(x)$ = 0.5	$\alpha(x)$ = 0.25	$\alpha(x)$ = 0.0
MOX	11.0147	0.116	0.044	0.006	-0.008
UO_2	12.6663	-0.296	-0.107	-0.012	0.019

errors near the material interface and the vacuum boundary are reduced by increasing the mixed region width to a certain value, at which point further increasing the width degrades the error reduction. In each case, the error in the interior of the MOX and UO_2 regions actually increases monotonically when using the mixed P_1-DP_0 approximation, although the error in those regions remains small. The optimal ERF set for the $\alpha(x)$ = 0.5 mixed P_1-DP_0 approximation occurs for a mixed region width of 0.7 mfp and the optimal set for the $\alpha(x)$ = 0.25 case occurs for a mixed region width of 0.4 mfp. Both of these optimal ERF sets are given in Table II. The total, interface, and boundary ERFs for the mixed P_1-DP_0 approximation with $\alpha(x)$ = 0.25 are clearly smaller than those for the $\alpha(x)$ = 0.5 case. Conversely, the ERFs for the interior of the MOX and UO_2 regions are greater than unity and larger for the $\alpha(x)$ = 0.25 case. Thus, the error in the total, interface, and boundary edit regions is decreased by using $\alpha(x)$ = 0.25 instead of $\alpha(x)$ = 0.5, while the error in the interior edit regions is increased. We note that with $\alpha(x)$ = 0.25, the RMS relative errors at the material interface and near the boundary are reduced by roughly a factor two. The total error is reduced by a similar amount. The error in the interior of the MOX region is increased by approximately 32% and in the interior of the UO_2 region by approximately 53%. However, the error in the interior of these regions remains small.

Figure 6 plots the RMS relative error in the scalar flux for the DP_0 angular approximation [$\alpha(x) = 0$ in the mixed region] for each of the five edit regions as a function of the number of mfp in the mixed region. These curves follow the same general trend as for the mixed P_1-DP_0 case, with a few differences. The optimal error reduction factor set for this case occurs at 0.225 mfp as opposed to 0.4 mfp for the $\alpha(x)$ = 0.25 P_1-DP_0 case. The optimal DP_0 error reduction factor set is given in Table II. We see that the optimal DP_0 error reduction factors for the total, interface, and boundary regions are even smaller than those

obtained using the mixed P_1-DP_0 approximation with $\alpha(x)$ = 0.25. The ERFs in the MOX and UO_2 regions are greater than unity and even larger. Figure 7 plots the total error reduction factor as a function of the interface/boundary width for both the mixed P_1-DP_0 and the DP_0 approximation. The mixed P_1-DP_0 approximation, particularly with $\alpha(x)$ = 0.25, exhibits the largest range over which significant error reduction occurs. In addition, we note that the standard DP_0 approximation method appears more susceptible to causing an overall *degradation* in accuracy (i.e. the error reduction factor is greater than unity for values of the mixed region width greater than approximately 1 mfp). Thus it appears, at least for this test problem, that the mixed P_1-DP_0 approximation is more robust than the standard DP_0 approximation for treating material interaces and vacuum boundaries.

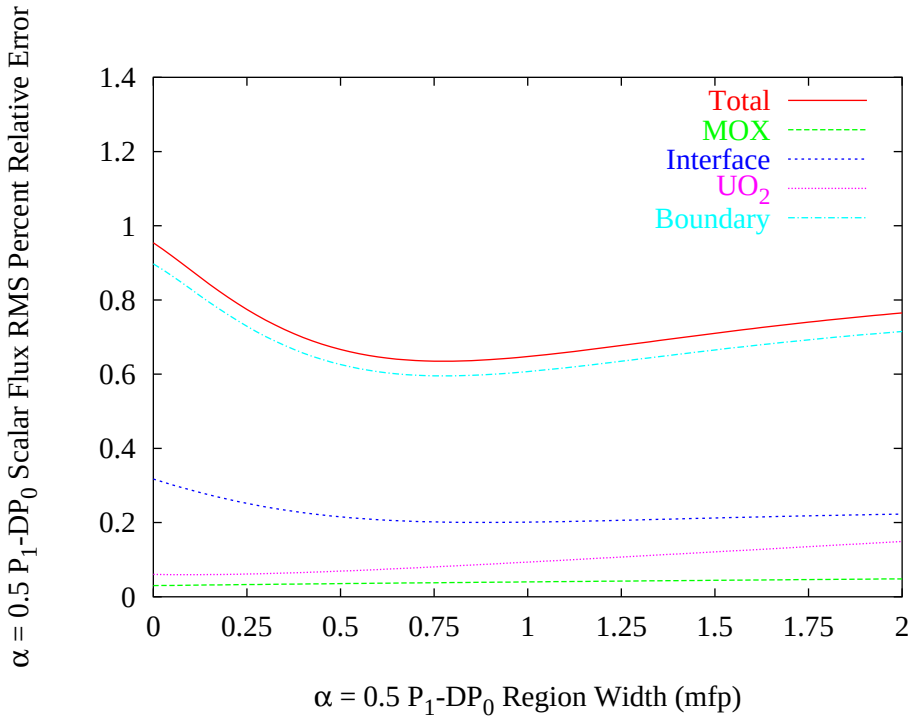

Figure 4. Edit Region Errors for $\alpha(x)$ = 0.5

Comparing the computed regional absorption rates from Table III, we see that the most accurate absorption rates are obtained using the mixed P_1-DP_0 approximation with $\alpha(x)$ = 0.25 in the mixed region. For that case, the error in the absorption rate is decreased by a factor of appoximately twenty in the MOX region and a factor of twenty-five in the UO_2 region.

Finally, in Figure 8 we plot the percent relative error in the scalar flux across the slab for the P_1 approximation and for the mixed P_1-DP_0 approximation with $\alpha(x)$ = 0.25 and $\alpha(x)$ = 0.0 (DP_0 approximation) using the respective optimal mixed region width. Significant accuracy improvements have clearly been obtained near the material interface and the vacuum boundary when using the mixed P_1-DP_0 approximation.

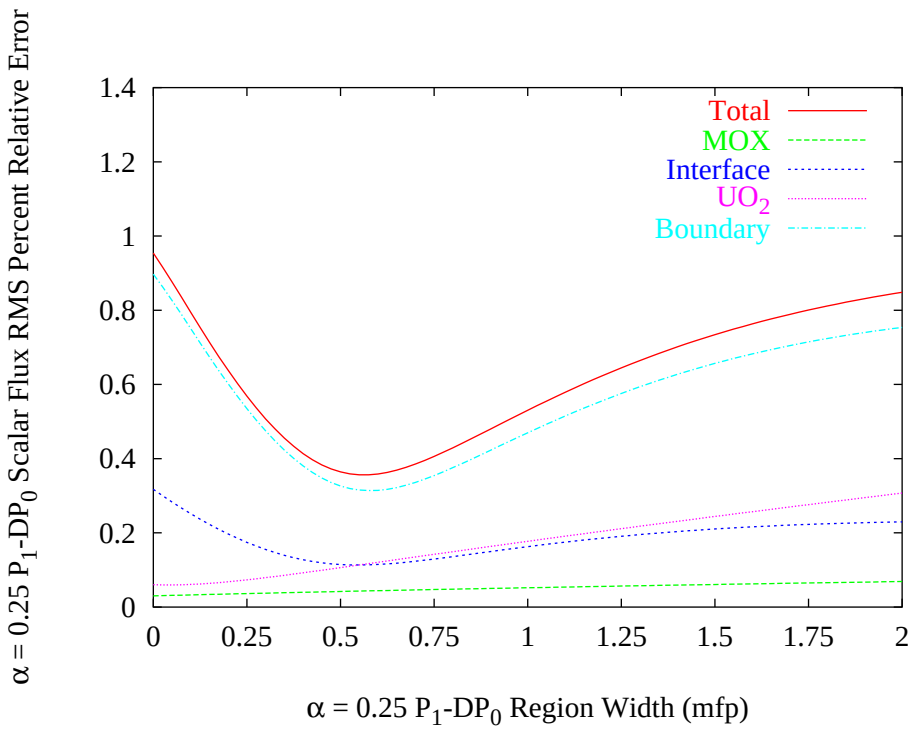

Figure 5. Edit Region Errors for $\alpha(x)$ = 0.25

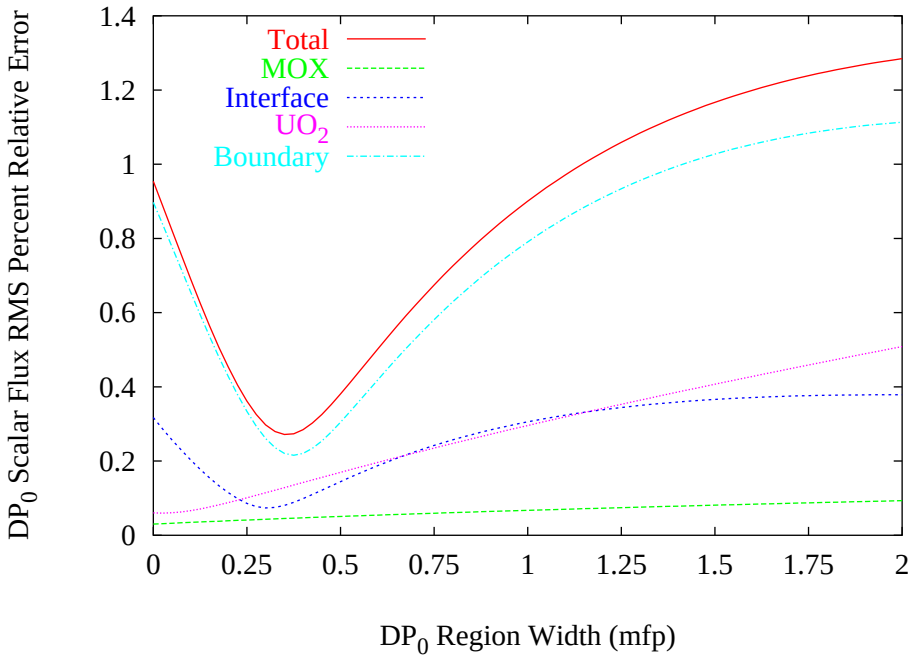

Figure 6. Edit Region Errors for DP_0

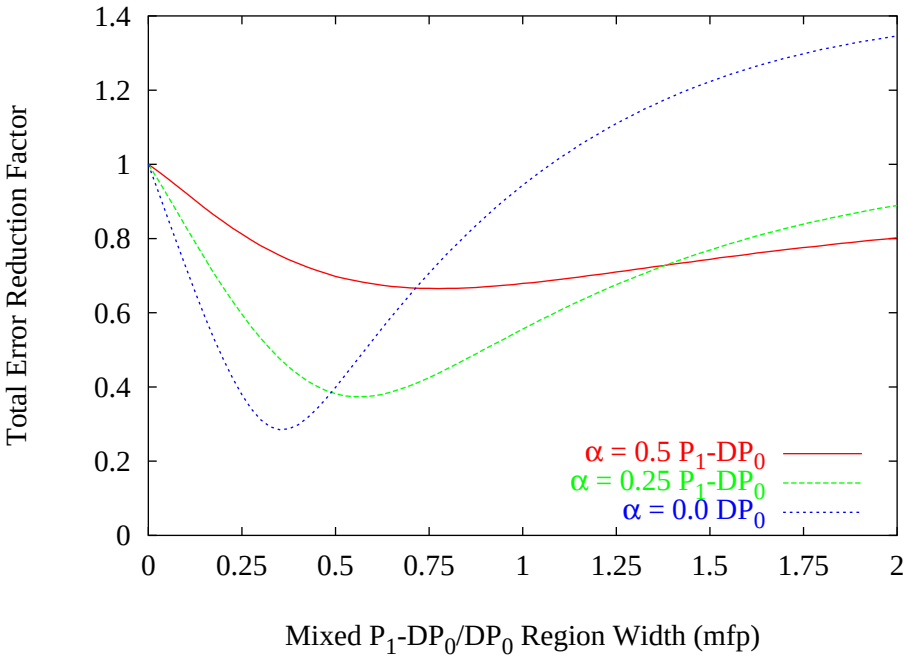

Figure 7. Total Error Reduction Factors

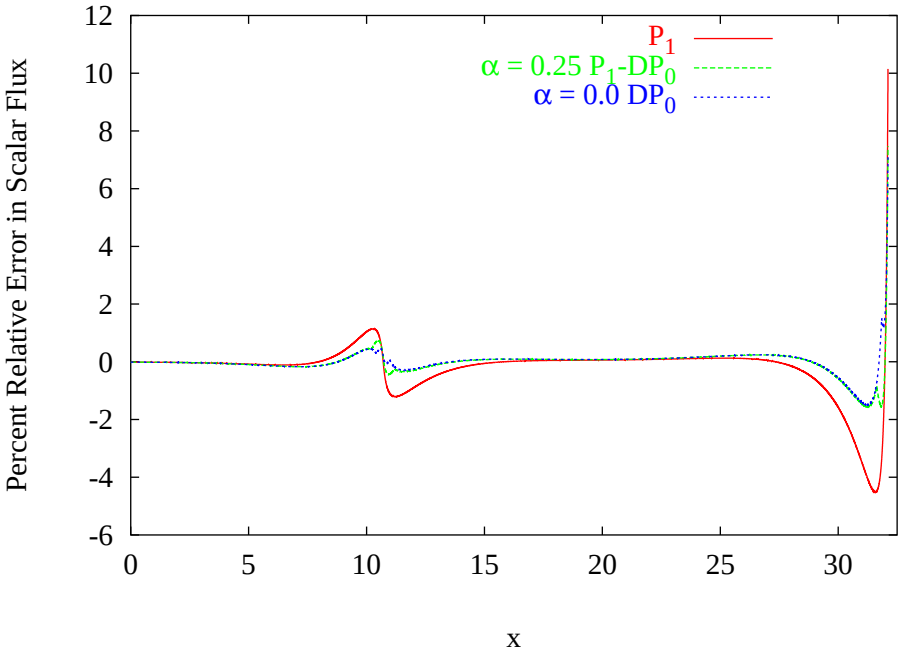

Figure 8. Percent Relative Error in the Scalar Flux

4. CONCLUSIONS

In this paper, we derived via a variational analysis a mixed P_1-DP_0 angular approximation to the time-independent monoenergetic neutron transport equation with linearly anisotropic scattering in one-dimensional planar geometry. This variational analysis shows that both the scalar flux and the current are continuous at material interfaces. Standard Marshak boundary conditions are also obtained via the variational analysis. The mixed angular approximation contains a space-dependent weight factor $\alpha(x)$ that controls the local angular approximation used. The diffusion theory obtained is identical to standard P_1 diffusion theory with the exception of the diffusion coefficient. The diffusion coefficient in the mixed P_1-DP_0 approximation contains the term $\alpha(x)$ which effectively interpolates between the standard P_1 and DP_0 definitions of the diffusion coefficient. The mixed P_1 diffusion theory requires essentially the same computational work as standard P_1 diffusion theory.

We applied the mixed P_1-DP_0 diffusion theory to the solution of a one-dimensional, two-region mixed-oxide fuel test problem. Our approach was to use the standard P_1 approximation everywhere in the system except near the material interface between the MOX and UO_2 regions and near the vacuum boundary. In those regions, we used either the mixed P_1-DP_0 approximation or a standard DP_0 approximation. The results show that more accurately treating the material interfaces and boundary conditions using these approximations gives significant accuracy improvements. The improvement in accuracy observed when using the standard DP_0 approximation is slightly better than that obtained using the mixed P_1-DP_0 approximation with $\alpha(x) = 0.25$. However, the mixed P_1-DP_0 approximation with $\alpha(x) = 0.25$ appears more robust than the standard DP_0 approximation and is therefore deemed the preferable choice.

Several areas of future work exist that we would like to pursue. First, the mixed P_1-DP_0 diffusion theory should be applied to a broader range of problems to determine if the results shown in this paper are representative. If so, it would be useful to extend the mixed P_1-DP_0 variational analysis to multiple dimensions following the approach of Paveri-Fontana and Amster [3]. Then the efficacy of treating material interfaces and vacuum boundaries using the mixed P_1-DP_0 approximation in multi-dimensional geometries could be evaluated. Next, we would also like to extend the variational analysis to obtain the mixed P_3-DP_1 approximation in planar geometry. If this approximation demonstrates improved accuracy, then we would like to consider the use of the mixed angular approximation treatment at material interfaces and vacuum boundaries with the simplified P_3 approximation in multiple dimensions. Finally, we would also like to consider using a similar methodology to a derive a mixed P_1-P_2 angular approximation. In this manner, it may be possible to take advantage of the improved accuracy of the P_2 approximation while avoiding its inherent scalar flux discontinuities present at material interfaces.

ACKNOWLEDGEMENTS

This work was performed under the auspices of the U.S. Department of Energy by the University of California Lawrence Livermore National Laboratory under contract No. W-7405-Eng-48.

REFERENCES

[1] B. Davison, *Neutron Transport Theory*, Oxford University Press, London England (1957).

[2] G.I. Bell and S. Glasstone, *Nuclear Reactor Theory*, Robert E. Krieger Publishing Co., New York (1970).

[3] S.L. Paveri-Fontana and H. Amster, "An Altered Diffusion Theory Based on the Double P-0 Approximation for All Geometries," *Nuc. Sci. Eng.*, **44**, pp. 44-57 (1971).

[4] A. Demény, K.M. Dede, and K. Erdei, "Spherical Harmonics Approximations of Neutron Transport," *Nuc. Sci. Eng.*, **61**, pp. 534-535 (1976).

[5] E. Gelbard, J. Davis, and J. Pearson, "Iterative Solutions to the P_ℓ and Double-P_ℓ Equations," *Nuc. Sci. Eng.*, **5**, pp. 36-4 (1959).

[6] R.P. Rulko, D. Tomašević, and E.W. Larsen, "Variational P_1 Approximations of General-Geometry Multigroup Transport Problems," *Nuc. Sci. Eng.*, **121**, pp. 393-404 (1995).

[7] P.S. Brantley and E.W. Larsen, "The Simplified P_3 Approximation," *Nuc. Sci. Eng.*, **134**, pp. 1-21 (2000).

[8] C. Cavarec, J.F. Perron, D. Verwaerde, and J.P. West, "Benchmark Calculations of Power Distributions Within Assemblies", HT-12/94006 A, NEA/NSC/DOC (94) 28, Nuclear Energy Agency Committee on Reactor Physics (1994).